

Iodine Perfusion Maps in Computed Tomographic Pulmonary Angiography: What Radiologists Need to Know?



Shu Yi Tan¹, Ken Lau^{1,2}, Adina Borsaru¹, Dana Jackson¹ and Dee Nandurkar^{1*}

¹Diagnostic Imaging, Monash Medical Centre, Australia

²Faculty of Medicine, Monash University, Australia

Submission: June 05, 2017; Published: August 23, 2017

*Corresponding author: Dee Nandurkar, Diagnostic Imaging, Monash Medical Centre, 246 Clayton Road, Clayton, VIC. 3168, Australia, Tel: +61395942200; Fax: +61395946693; Email: nandurkar.dee@gmail.com

Abstract

Computed tomographic pulmonary angiography is the gold standard in diagnosing pulmonary embolism (PE). There is increasing use of dual energy CT (DECT) scanners in producing iodine perfusion maps. These maps assist in diagnosing a PE. However, many conditions can mimic perfusion defects on iodine maps including artefacts, pleural effusion, pulmonary artery compression, emphysema, vasculitis, pulmonary collapse, interstitial lung disease, MacLeod syndrome, mosaic perfusion and lung masses. It is important for the radiologist to familiarize themselves with these conditions to avoid misinterpreting iodine perfusion maps.

Keywords: CT pulmonary angiogram; Dual energy CT; Iodine map; Pulmonary embolism; Perfusion defect

Introduction

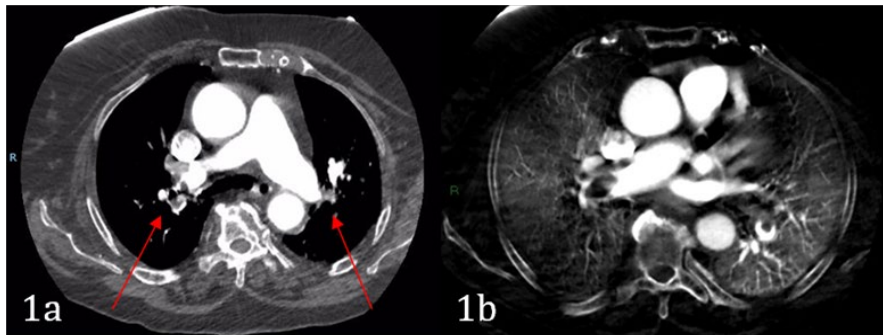


Figure 1: Occlusive PE in the right upper and left lower lobes on mediastinal window (1a) and associated perfusion defect on iodine map (1b).

Computed tomographic pulmonary angiography (CTPA) has become the mainstay in diagnosis of pulmonary embolism [1]. The advent of DECT has enabled simultaneous acquisition of datasets at two energy spectra; commonly at 80 KVp and 140 KVp. Iodine perfusion maps are generated using the concept of material decomposition, difference in attenuation at different energies [2]. Iodine attenuation is significantly greater at 80 KVp compared to 140 KVp resulting in derivation of an iodine map, representing distribution of iodinated contrast within the lung parenchyma which reflects the perfusion status of the lung [3]. Pulmonary perfusion map may aid the diagnosis of PE, as some emboli, in particular the occlusive type, can lead to perfusion

deficits, commonly depicted as well demarcated wedge shaped defects. Perfusion defects detected on iodine maps are, however, not specific to embolic etiology; with vascular compression and diseases, artefact, airways disease and primary pulmonary parenchymal pathology also resulting in perfusion defects [4]. On the contrary, certain lesions in lungs may have increased vascular perfusion and may be seen as increased iodine concentration on iodine maps.

The aim of this pictorial review is to demonstrate the appearances of some common pulmonary Pathologies which can mimic PE on iodine maps created from DECT.

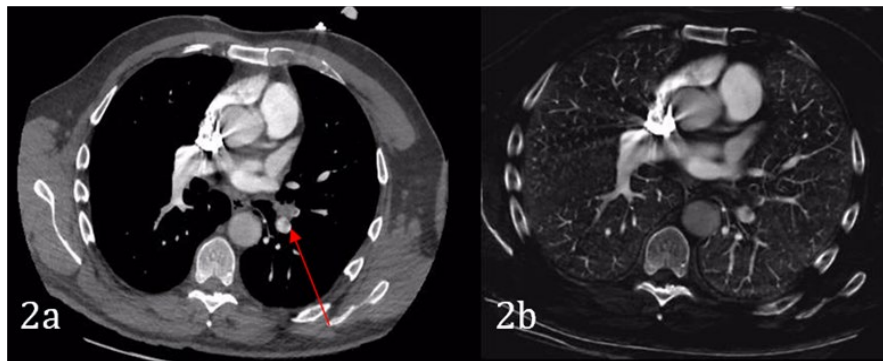


Figure 2: Non-occlusive left sided PE on mediastinal window (2a) with no associated perfusion defect on iodine map (2b).

Discussion

Pulmonary embolism

Occlusive emboli: The perfusion defects associated with PE on iodine map tend to be wedge-shaped and at the periphery of lungs, particularly if the occlusions are above the segmental level. DECT depicted perfusion defects from PE on iodine maps are generally in good agreement with scintigraphic perfusion findings [5]. Presence of occlusive PE correlates well with

segmental/subsegmental perfusion defects on iodine maps¹. Therefore, absence of perfusion defects confers a high negative predictive value in excluding occlusive emboli. Fink et al. [3] have reported sensitivity and specificity of DECT for detection of PE on a per segment basis as 100%. In comparison, CT angiography has a sensitivity and specificity of 60-66.7% and 99.5-8% respectively. A study by Wu et al. [6] found that all patients with occlusive PE were accurately detected on perfusion maps (Figure 1).

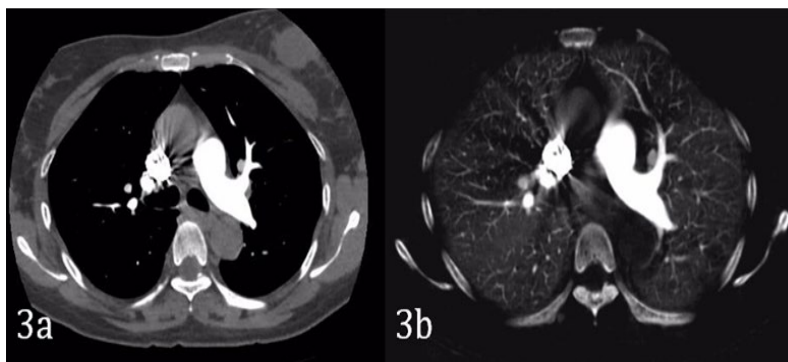


Figure 3: Beam hardening artefact on mediastinal window (3a) and iodine map.

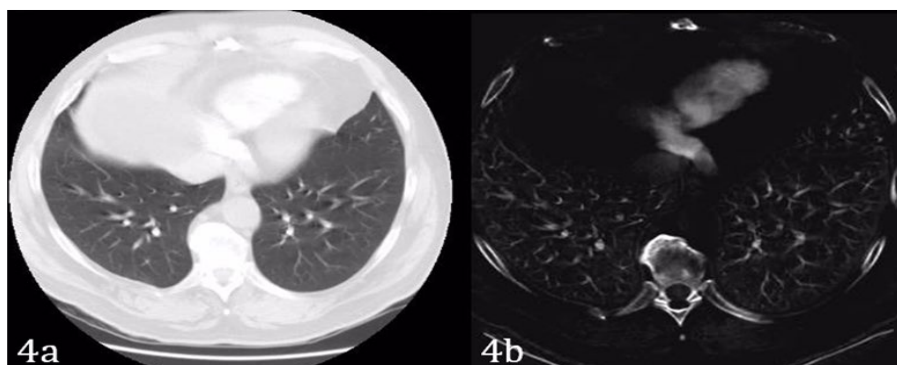


Figure 4: Respiratory motion artefact on lung window (4a) resulting perfusion defect on iodine map (4b).

Non-occlusive emboli: Non-occlusive PE are poorly associated with perfusion defects [7]. Only 2 out of 33 non-occlusive clots in the study by Thieme et al. [7] had perfusion defects and 11 out of 42 non-occlusive emboli have defects on iodine maps¹ (Figure 4).

Beam hardening artifact

Dense contrast in the superior vena cava or the brachiocephalic vein results in beam hardening artifact which in turn causes apparent defects across the upper lungs which are

band-like². Other patterns such as crescentic, polygonal and ovoid shapes have also been described with the defects exhibiting sharp margins. These are typically observed in the apical and anterior segment of the right upper lobe and the apico-posterior

and lingular segments of the left upper lobe [7]. Artefacts can be reduced by caudocranial scan direction with reduction of the amount of iodinated contrast in central veins and by relatively lower contrast flow [1] (Figure 5).

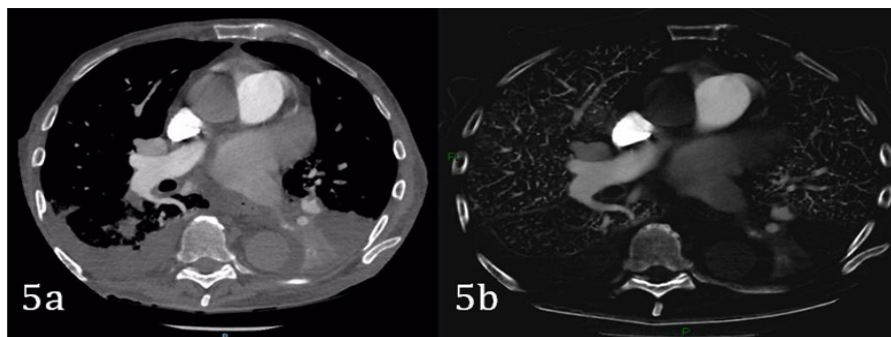


Figure 5: Pleural effusion on mediastinal window (5a) and iodine map (5b).

Motion artifact

Motion artifact resulting from cardiac and diaphragmatic movement results in artifacts in the right middle lobe, lingular segment of the left upper lobe and the lung bases [2]. The diaphragmatic motion results in apparent curvilinear defects on iodine map. Blurred contours on the mediastinal and lung windows may help to distinguish these artifact from true perfusion artifact associated with PE.

Pleural effusion

Defect created by pleural effusion iodine map is easily recognized by its crescentic peripheral contour which is

concordant with the distribution of pleural fluid. It can also be easily confirmed by reviewing the mediastinal window settings on the CTPA study.

Pulmonary artery compression

External pulmonary arterial compression also yields perfusion defects on iodine maps. Conglomerate nodal or neoplastic mass centrally that compresses or invades the proximal pulmonary artery may result in peripheral wedge shaped perfusion defect on iodine map (Figure 6). Fibrosing mediastinitis causing pulmonary arterial compression has also been demonstrated to yield wedge shaped perfusion defects⁴.

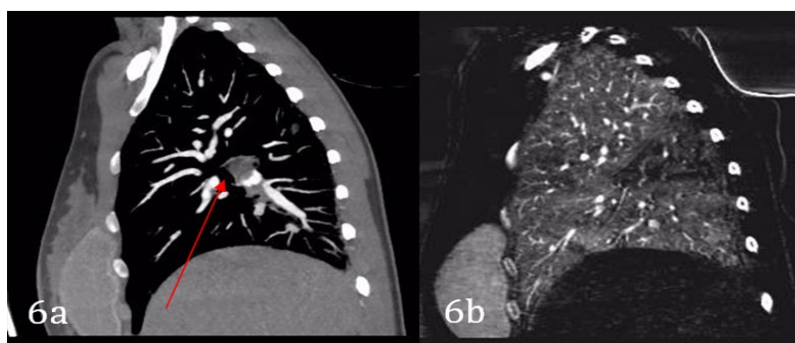


Figure 6: Pulmonary artery compression on mediastinal window (6a) and associated iodine map defect (6b).

Vasculitis

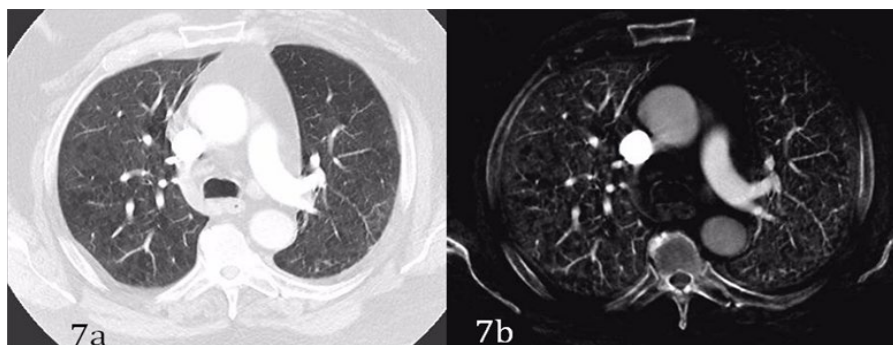


Figure 7: Emphysema on lung window (7a) and associated non-segmental perfusion defect (7b).

Although there are no cases in our patient group. Hypothetically, vasculitis involving the pulmonary arteries will

result in reduced pulmonary arterial caliber and subsequently reduced perfusion within the lungs (Figure 7).

Emphysema

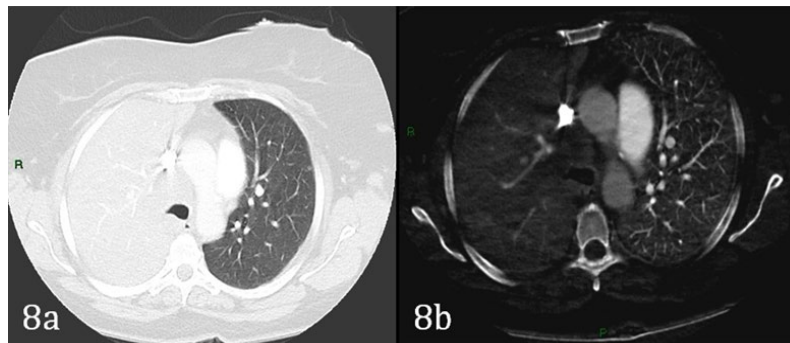


Figure 8: Lung collapse on lung window (8a) and perfusion defect on iodine map (8b).

The emphysematous lung by virtue of lung destruction and paucity of pulmonary parenchyma and vasculature demonstrates deficient iodine content and as a result, perfusion defects on iodine map. These defects do not conform to the segmental

anatomy, but correspond to the extent of emphysema on lung window settings of a CTPA. The degree of perfusion reduction generally correlates well with the degree of emphysema [8] (Figure 8).

Pulmonary collapse

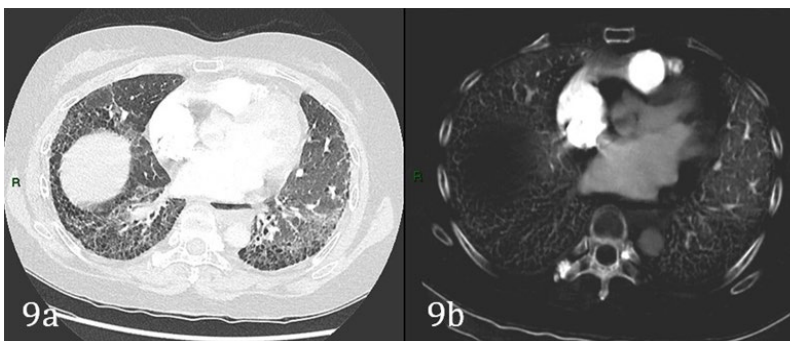


Figure 9: Pulmonary fibrosis in lung window (9a) with associated perfusion defect (9b).

Pulmonary collapse results in altered perfusion with defect on iodine map paralleling the distribution of the pulmonary collapse and is readily recognized on CT images. Material decomposition required in order to obtain perfusion maps need

pulmonary parenchymal density between -960 to -600 HU². As the density of the collapsed lung falls outside this range, perfusion defects result due to technical failure to produce a perfusion map² (Figure 9).

Interstitial lung disease

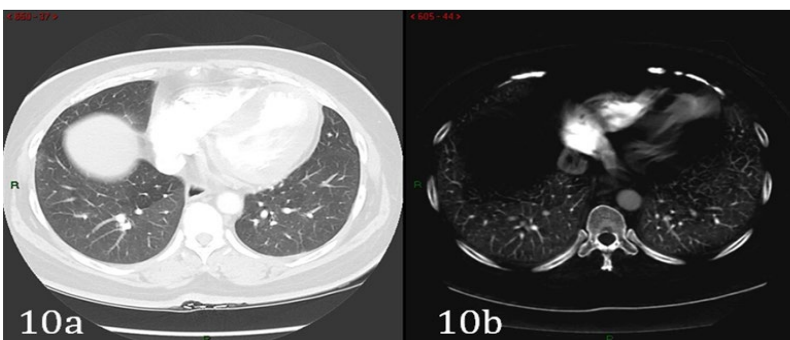


Figure 10: Air trapping in lung window (10a) with associated mosaic perfusion on iodine map (10b).

Interstitial lung disease results in non-segmental perfusion map defects conforming to the distribution of pulmonary fibrosis. Ventilation perfusion mismatch is the commonest scintigraphic pattern seen on V/Q scans in patients with idiopathic pulmonary

fibrosis. The cause is vascular destruction by the fibrotic process rather than vasculitis per se [9]. SPECT images have also demonstrated that the perfusion defects on scintigraphy were associated with regions of cystic air spaces shown on CT

scans, the “honeycomb” lung pattern. Hence, this also explains the perfusion defects evident on iodine maps in patients with pulmonary fibrosis. Density of the fibrotic lung falls outside the

Mosaic perfusion

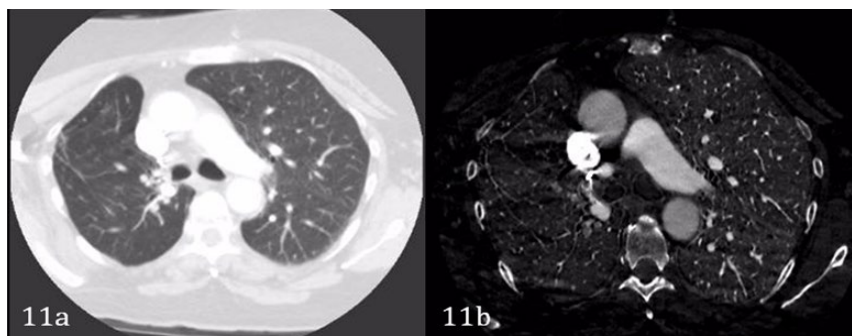


Figure 11: McLeod syndrome with relative hypolucency of right lung (11a) with associated perfusion defect (11b).

Mosaic pattern may result from small airways disease related air trapping or pulmonary vascular disease. Various vascular disease such as PE and vasculitis can result in mosaic attenuation. Regional hypoxia from small airways disease such as asthma produces patchy areas lung with differing attenuation. This can also further result in secondary vasoconstriction. Both phenomenon can produce defects on iodine maps (Figure 11).

MacLeod syndrome

Swyer-James-MacLeod syndrome is a post-infective state resulting in destruction of the bronchiole. Radiographically, it is characterized by unilateral hyperlucent lung which may be normal or reduced in size with diminished lung and vascular markings and a mediastinal shift to the affected side on inspiration which swings to the contralateral side during expiration suggesting air trapping in the affected lung. The pulmonary artery in these

range required for material decomposition resulting in perfusion defects [2] (Figure 10).

patients is also markedly diminished in size with near complete absence of perfusion on ventilation/perfusion scintigraphy [10]. These changes are similarly reflected on the iodine perfusion map with extensive deficient perfusion on the affected side.

Lung Mass

Chae et al. [11] demonstrated that DECT has the ability to generate virtual non contrast and contrast enhanced images from a single post contrast acquisition and measure the degree of contrast enhancement without additional radiation. Statistically significant difference was demonstrated in the absolute density and degree of enhancement using DECT between benign and malignant pulmonary nodules, with malignant nodules exhibiting higher density and degree of enhancement. This is demonstrated in the images (Figure 12).

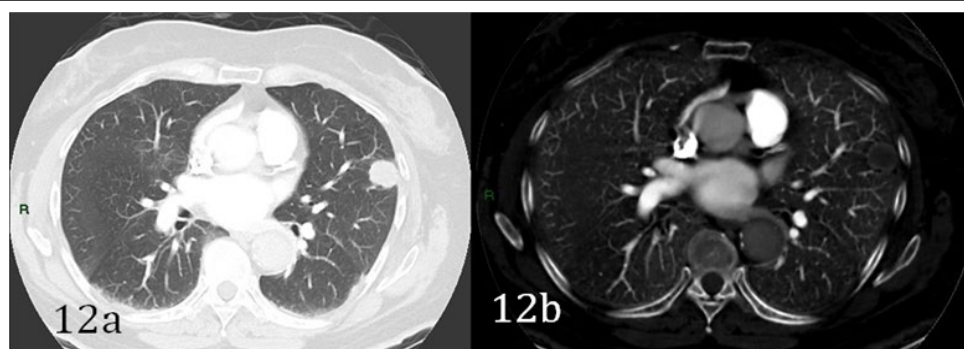


Figure 12: Pulmonary mass on lung window (12a) and increased density peripherally and reduced perfusion centrally on iodine map (12b).

A strong correlation has also been demonstrated between the SUV max and maximum iodine-related attenuation in non-small cell than small cell lung cancer. Differences in tumour biology and different angiogenic factors between the two different histologic subtypes are some of the proposed explanations for these differences [12].

Conclusion

Iodine maps generated using DECT scanners are increasingly used to aid image interpretation of CTPA studies. Whilst

presence of perfusion defects on iodine map would suggest the presence of occlusive PE, these may also be encountered in a multitude of conditions. Absence of perfusion abnormality does not exclude a non-occlusive PE. The iodine maps themselves are also subject to multiple artifacts and are variably affected by many of the commonly encountered parenchymal pulmonary pathologies and pulmonary lesions which would require proper CT characterization. As the use of DECT increases, reporting radiologists would need to familiar with the manifestations of lung pathologies, apart from PE, on the iodine perfusion maps.

Conflict of Interest

The authors declare that there is no conflict of interest in the production of this manuscript.

References

1. Thieme SF, Johnson TRC, Lee C, McWilliams J, Becker CR, et al. (2009) Dual energy CT for assessment of contrast material distribution in the pulmonary parenchyma. *AJR* 193(1): 144-149.
2. Kang MJ, Park CM, Lee CH, Goo JM, Lee HJ (2010) Dual energy CT: clinical applications in various pulmonary diseases. *Radiographics* 30(3): 685-698.
3. Fink C, Johnson TR, Michaely HJ, Morhard D, Becker C, et al. (2008) Dual energy CT angiography of the lung in patients with suspected pulmonary embolism: initial results. *Rofo* 180(10): 879-883.
4. Kim BH, Seo JB, Chae EG, Lee HJ, Hwang HJ, et al. (2012) Analysis of perfusion defects by causes other than acute pulmonary thromboembolism on contrast enhanced dual energy CT in consecutive 537 patients. *Eur J Radiol* 81(4): 647-652.
5. Thieme SF, Becker CR, Hacker M, Nikolaou K, Reiser MF, et al. (2008) Dual energy CT for assessment of lung perfusion-correlation to scintigraphy. *Eur J Radiol* 68(3): 369-374.
6. WU WH, Cheng JJ, Li JY, Yin Y, Hua J, et al. (2012) Pulmonary embolism detection and characterization through quantitative iodine based material decomposition images with spectral computed tomography imaging. *Investigative radiology* 47(1): 85-91.
7. Kang MJ, Park CM, Lee CH, Goo JM, Lee HJ (2010) Focal iodine defects on color coded iodine perfusion maps of dual energy CT pulmonary angiographic images: a potential diagnostic pitfall. *AJR* 195(5): W325-W330.
8. Pansini V, Remy-Jardin M, Faivre JB, Schmidt B, Dejardin-Bothelo A, et al. (2009) Assessment of lobar perfusion in smokers according to the presence and severity of pulmonary emphysema: preliminary experience with dual energy CT angiography. *Eur Radiol* 19(12): 2834-2843.
9. Strickland NH, Hughes JMB, Hart DA, Myers MJ, Lavender JP (1993) Cause of regional ventilation-perfusion mismatch in patients with idiopathic pulmonary fibrosis. A combined Ct and scintigraphic study. *AJR* 161(4): 719-725.
10. Gottleib LS, Franklin T (1976) Swyer-James (Macleod's syndrome) variations in pulmonary-bronchial arterial blood flow. *Chest* 69(1): 62-66.
11. Chae EJ, Song JW, Seo JB, Krauss B, Jang YM, et al. (2012) Clinical utility of dual-energy CT in the evaluation of solitary pulmonary nodules: Initial experience. *Radiology* 249(2): 671-681.
12. Lu GM, Zhao Y, Zhang LJ, Schoepf UJ (2012) Dual-energy CT of the lung. *AJR* 199(5): S40-S53.



This work is licensed under Creative Commons Attribution 4.0 License
DOI: [10.19080/CTCMI.2017.02.555577](https://doi.org/10.19080/CTCMI.2017.02.555577)

Your next submission with Juniper Publishers will reach you the below assets

- Quality Editorial service
- Swift Peer Review
- Reprints availability
- E-prints Service
- Manuscript Podcast for convenient understanding
- Global attainment for your research
- Manuscript accessibility in different formats
(Pdf, E-pub, Full Text, Audio)
- Unceasing customer service

Track the below URL for one-step submission

<https://juniperpublishers.com/online-submission.php>